ChemElectroChem

Research Article
doi.org/10.1002/celc.202300821

Chemistry Europe
European Chemical Societies Publishing

www.chemelectrochem.org

Efficient Electrocatalytic H_2 Production by Immobilized Co(III)-myoglobin

Mirco Meglioli,[a] Giulia Di Rocco,[b] Antonio Ranieri,[b] Carlo Augusto Bortolotti,[b] Marco Sola,[b] Gianantonio Battistuzzi,*[a] and Marco Borsari*[a]

The thermodynamics and kinetics of heterogeneous electron transfer (ET) for Co-substituted horse myoglobin (Co–Mb) and its derivatives with ammonia and imidazole as heme axial ligands were studied with cyclic voltammetry on a pyrolytic graphite electrode along with their ability to mediate the electro-catalytic production of H_2. All the proteins experience a non-diffusive electrochemical regime as electrode-bound species. The adsorbed Co–Mb construct carries out the electrocatalytic reduction of water protons to H_2 with a good efficiency under anaerobic conditions thus yielding a simple and tunable system for H_2 production. Replacement of H_2O as Co axial ligand by ammonia and imidazole significantly lowers the catalytic currents for H_3O^+/H_2O reduction to H_2. The E°′ values of the Co(III)/Co(II) redox couple for all species are mainly determined by the enthalpic contribution. Differences were found in the kinetics of ET for the different protein adducts due to changes in the activation enthalpies. However, all species share the same distance of about 14 Å from the electrode surface to the Co(III)/Co(II) center determined using the Marcus model, consistent with a non-denaturing adsorption of the protein.

Introduction

Alternatives to fossil fuels are highly sought after for obvious climatic, economic and social reasons. One of the viable options is the large-scale production of dihydrogen. Indeed, H_2 *(i)* is one of the carriers with the highest energy density per unit mass, *(ii)* produces water as a result of oxidation, *(iii)* can exploit infrastructures already available, *(iv)* is potentially inexhaustible and *(v)* can be used by conventional thermic engines.[1,2] Currently, H_2 is produced by steam reforming of hydrocarbons, which presents obvious sustainability problems, or by water electrolysis, whose main problem is the high overvoltage for the discharge of H_2, which significantly increases the energy required for the reaction. This issue is further compounded by the low efficiency of the solar panels used to produce the electricity needed for the process. Nevertheless, electrochemical production of H_2 is much more sustainable than steam reforming. Recently, research has moved towards the production of hydrogen by enzyme-catalyzed reactions. These processes are inspired by the metalloproteins hydrogenases, which catalyze the reversible conversion of dihydrogen into protons and electrons:[3–6]

$$H_2\ (\rightleftharpoons H^+ + H^-) \rightleftharpoons 2\ H^+ + 2\ e^-$$

The breaking of the hydrogen molecule occurs thanks to the increase in acidity of the active site that induces a heterolytic rupture of the H–H bond, while the reverse reaction involves the binding of a hydride ion and an H^+ ion.[4] Hydrogenases are widespread in nature and are classified as [NiFe], [Fe], [FeFe] hydrogenases, according to the metal ions forming the active site. They also contain an iron-sulfur cluster which serves as an electron transfer center. Although the catalytic activity of these enzymes is very high,[3,4,7] they are very sensitive to ROS and become inactive in the presence of dioxygen, which reacts with the metal center.[4,6] Therefore, attempts have been made to exploit biomimetic systems containing common transition metals imparted with hydrogenase activity, working under aerobic conditions.[4,5,8] Cobalt (III/II) is one of the best candidates in this respect as it lowers the overvoltage needed for hydrogen reduction and may work in the presence of dioxygen.[6] Some Co-coordination compounds, such as cobaloximes, have shown such peculiar catalytic activity mainly in non-aqueous solutions[5,6,9] under aerobic conditions,[3] while proved not to be particularly effective in neutral aqueous medium. One viable strategy to improve the solubility and catalytic activity in an aqueous environment is the synthesis of compounds in which the catalytically active Co-center is embedded into a simplified protein scaffold, consisting of the aminoacidic portion of the active site of the protein.[10,11] This approach resulted in several biomimetic catalysts, such as cobalt-peptides[3,7,12–14] and PSI-cobaloxime complexes,[12] capable of acting through electro-catalytic and photocatalytic pathways. Despite substantial

[a] *M. Meglioli, G. Battistuzzi, M. Borsari*
Department of Chemical and Geological Sciences, University of Modena and Reggio Emilia, via Campi 103, 41125 Modena, Italy
Phone: +39-0592058642
E-mail: gianantonio.battistuzzi@unimore.it
marco.borsari@unimore.it

[b] *G. Di Rocco, A. Ranieri, C. A. Bortolotti, M. Sola*
Department of Life Sciences, University of Modena and Reggio Emilia, via Campi 103, 41125 Modena, Italy

progress, most of these biomimetic compounds still show poor solubility in water and require organic solvents to accomplish their catalytic activity.[10,15–17] An alternative strategy consists in replacing the heme group (Fe-porphyrin) naturally present in heme-proteins, with the corresponding Co-derivative, in order to produce Co-substituted metallo-enzymes catalyzing the production of H_2.[12,18] These systems show a high solubility in water, resistance to degradation reactions and can be engineered to control the reactivity by selected point mutations.[6,9,12,18–25]

In this work, we have studied the ability of Co-substituted horse myoglobin (Mb), obtained by replacing the native heme group with cobalt-protoporphyrin IX, to catalyze the electrochemical reduction of water to H_2. Mb was chosen because the metal ion is coordinated by the nitrogen atoms of the tetrapyrrole ring and the proximal His93 nitrogen and the open distal axial coordination position can bind exogenous molecules.[6,9] Moreover, replacement of the metal center is facilitated by the absence of covalent linkages between the heme group and the protein matrix. The capacity of Co–Mb to catalytically reduce water to H_2 in an electrochemical environment was studied at different pH and temperature values in aqueous solution and in the presence of nitrogenous exogenous heme axial ligands (NH_3 and imidazole) to test the effect of the occupancy of the distal axial coordination position on the catalytic efficiency. It turns out that the presence of the labile axial water instead of a stronger N-donor ligand facilitates the catalytic reduction of H^+ to H_2 although the electron transfer process is faster in the presence of the axial imidazole ligand.

Experimental

Materials

Horse skeletal muscle myoglobin (Mb) was purchased from Sigma-Aldrich. Cobalt protoporphyrin IX was purchased from Porphyrin Systems Hombrecher e.K. (Halstenbek, Germany). Sodium monohydrogen phosphate, sodium di-hydrogen phosphate, sodium chloride, sodium perchlorate, hydrochloric acid, sodium hydroxide and ethyl methyl ketone (Carlo Erba Reagenti) were reagent grade. Tris and pyridine (PanReac AppliChem) were molecular biology and synthesis grade, respectively. Sodium dithionite (Sigma-Aldrich) was reagent grade. Purified water (Milli-Q Plus Ultrapure Water System coupled with an Elix-5 Kit by Millipore) was used throughout. The water resistivity was over 18 MΩ cm.

Co-Myoglobin Preparation

Lyophilized horse skeletal muscle myoglobin (Mb hereafter) was dissolved in 50 mM Tris buffer, pH 7.0 and the obtained solution was centrifuged at 11000 rpm for 10 minutes using Beckman Coulter AllegraTM V-15R centrifuge, to remove the undissolved fraction. Mb concentration was estimated from the Soret electronic absorption band by using a molar extinction coefficient $\varepsilon_{409} = 160000\ M^{-1}cm^{-1}$. Apo-Mb was obtained by solvent extraction with ethyl methyl ketone[19,20] at 0 °C at neutral pH. To eliminate possible traces of ethyl methyl ketone, the solution containing apo-Mb was dialyzed against two batches of 1 L of 50 mM Tris buffer pH = 8.0 at 4 °C for 3 hours and then centrifuged at 11000 rpm for 5 minutes. To verify iron protoporphyrin IX removal, the electronic absorption spectrum of the dialyzed solution was recorded. Reconstitution of holo-Mb with cobalt protoporphyrin IX was carried out with a slight modification of the published procedures.[21] Cobaltic protoporphyrin IX was dissolved in a mixture of water and pyridine 1:1 and then a slight excess of sodium dithionite was added to reduce Co(III) to Co(II). The solution of cobaltous protoporphyrin IX was added anaerobically to that of Apo-Mb to achieve a Co/Apo-Mb stoichiometric ratio of 2:1 and kept at 4 °C overnight. The solution was concentrated using an Amicon™ stirred ultrafiltration cell and then loaded onto a Sephadex™ G-15 gel-filtration column connected to an AKTA Prime chromatographic system and equilibrated with 50 mm phosphate buffer pH = 7.0 plus 0.1 M NaCl, to eliminate unbound Co-protoporphyrin IX. Fractions containing Co–Mb were collected and concentrated in an Amicon™ stirred ultrafiltration cell.

Electronic Absorption and MCD Spectra

Electronic absorption and MCD spectra of Co–Mb and its NH_3 and imidazole derivatives (see below) were recorded using a Jasco J-810 spectropolarimeter using a quartz cuvette of 0.5 cm path length. All experiments were carried out at 25 °C with protein solutions freshly prepared before use in 5 mM phosphate buffer and 50 mM sodium perchlorate at pH 7.2. The magnetic field for MCD measurements was provided by a GMW Magnet system Model 3470 split coil superconductivity magnet with a maximum field of 1 Tesla (T). MCD spectra were measured in θ = mdeg and converted to $\Delta\varepsilon$ [$M^{-1}cm^{-1}T^{-1}$] using the conversion factor $\Delta\varepsilon = \theta/(32980 \cdot c \cdot d \cdot B)$, where c is the protein concentration, B is the magnetic field (1 T), and d is the thickness of the sample (path length, 0.5 cm).[26–28]

Electrochemical Measurements

Cyclic voltammetry (CV) experiments were performed with a Potentiostat/Galvanostat mod. 273A (EG&G PAR, Oak Ridge, USA) using a cell for small volume samples (1.5 mL) under argon. A pyrolytic graphite (PG) electrode, a platinum ring, and a Standard Calomel Electrode (SCE) were used as working, counter, and reference electrode, respectively. The chemical-mechanical procedure for cleaning the working electrode surface consisted in the following steps: polishing with alumina slurry and final rinsing with distilled water for 2 min; the electrode was then subjected to 15 electrochemical cycles from −0.6 V to +0.3 V vs. SCE in 1 M H_2SO_4 and finally rinsed with purified water. All the applied potentials and $E^{\circ\prime}$ values reported in this work are referred to the standard hydrogen electrode (SHE), unless otherwise specified. The CVs were carried out using solutions containing 3 μM Co–Mb (determined spectrophotometrically) plus 5 mM phosphate buffer and 50 mM sodium perchlorate as base electrolyte at different pH values. The adducts of Co–Mb with NH_3 and imidazole were obtained upon addition of 1.2 mM NH_4Cl (which yields a NH_3 concentration of approximately 8 μM at pH 7.2) and 1.2 mM imidazole, respectively. UV-vis spectra indicate that these ligand concentrations warrant formation of the protein-ligand adducts. Electrochemical measurements were also performed on Cobalt protoporphyrin IX at pH 7.2, its solubility at pH 7.2 was detected spectrophotometrically and resulted about 2 μM.

Formal potentials $E^{\circ\prime}$ were calculated as the semi-sum of the anodic and cathodic peak potentials and resulted almost independent of scan rate (ν) in the range 0.02–0.5 Vs^{-1}. The experiments were repeated at least five times and the $E^{\circ\prime}$ values were found to be reproducible within ±0.002 V. The CV experiments at different temperatures were carried out with a "non-isothermal" cell in which

the reference electrode was kept at constant temperature (21 ± 0.1 °C) in a 1 M $NaClO_4$/Agar salt bridge while the half-cell containing the working electrode and the Vycor® (PAR) junction to the reference electrode was under thermostatic control with a water bath. The temperature was varied from 5 to 45 °C. With this experimental configuration, the standard entropy change ($\Delta S^{\circ\prime}_{rc}$) is given by:

$$\Delta S^{\circ\prime}_{rc} = S^{\circ\prime}_{red} - S^{\circ\prime}_{ox} = nF\ (dE^{\circ\prime}/dT) \quad (1)$$

Thus, $\Delta S^{\circ\prime}_{rc}$ was determined from the slope of the plot of $E^{\circ\prime}$ versus temperature which turns out be linear under the assumption that $\Delta S^{\circ\prime}_{rc}$ is constant over the limited temperature range investigated.[29–31] The enthalpy change ($\Delta H^{\circ\prime}_{rc}$) was obtained from the Gibbs-Helmholtz equation, namely as the negative slope of the $E^{\circ\prime}/T$ versus 1/T plot. Repeated cycling does not affect the voltammograms from 5 to 45 °C, indicating that the protein monolayer is stable. The non-isothermal behavior of the cell was carefully checked by determining the $\Delta H^{\circ\prime}_{rc}$ and $\Delta S^{\circ\prime}_{rc}$ values of the ferricyanide/ferrocyanide couple.[29,30]

The peak current for the immobilized protein turns out to be linear with the scan rate (see below), as expected for a diffusionless electrochemical process. The surface coverage Γ_0 for the immobilized electrochemically active protein was calculated from the overall charge Q_{tot} exchanged by the protein (determined upon integration of the baseline-corrected cathodic peaks) and the area A of the PG electrode by applying the relationship:

$$\int i(E)\ dE = \nu(nFA\Gamma_0) = \nu Q_{tot}$$

where ν is the scan rate (in Vs^{-1}), n (=1) the number of electrons exchanged in the redox reaction, and F is the Faraday constant. The area of the electrode was determined electrochemically using the Randles-Sevçik equation to the reduction peak of ferrocenium tetrafluoborate of known concentration in aqueous solution. The surface coverage for the Co–Mb and its NH_3 and imidazole adducts was found to range between 14 and 18 pmol/cm^2, similar to that reported for cytochromes *c* under similar conditions.[32–35] CVs at different scan rates (from 0.02 to 0.5 Vs^{-1}) were recorded to determine the rate constant k_s for the ET process of the adsorbed protein, using the Laviron method.[36] The effects of uncompensated cell resistance were minimized using the positive-feedback iR compensation function of the potentiostat, set at a value slightly below that at which current oscillations emerge. The separation between the anodic and the cathodic peak increases with increasing the scan rate, while the $E^{\circ\prime}$ values are unchanged. The k_s values were averaged over five measurements with and associate error of about 10%. The k_s values were measured in the range 5–45 °C to determine the activation enthalpies ($\Delta H^{\#}$) using the Arrhenius equation, namely from the slope of the plot of ln k_s versus 1/T. The catalytic efficiency of the proteins for H_2 development were measured by evaluating the shifts of the onset potential and H_2 reduction current densities at different pH values.

ResultsElectronic Absorption and MCD Spectra of Co^{3+}-Mb and its Imidazole and Ammonia Adducts

The electronic absorption spectrum of Co(III)-Mb features a symmetric Soret band at 424 nm, while the α and β bands are observed at 567 nm and 533 nm, respectively (Figure 1A). The spectrum coincides with those previously reported,[23] indicating the presence of a low-spin hexacoordinate Co^{3+} with the proximal histidine and a water molecule as axial ligands. The MCD spectrum

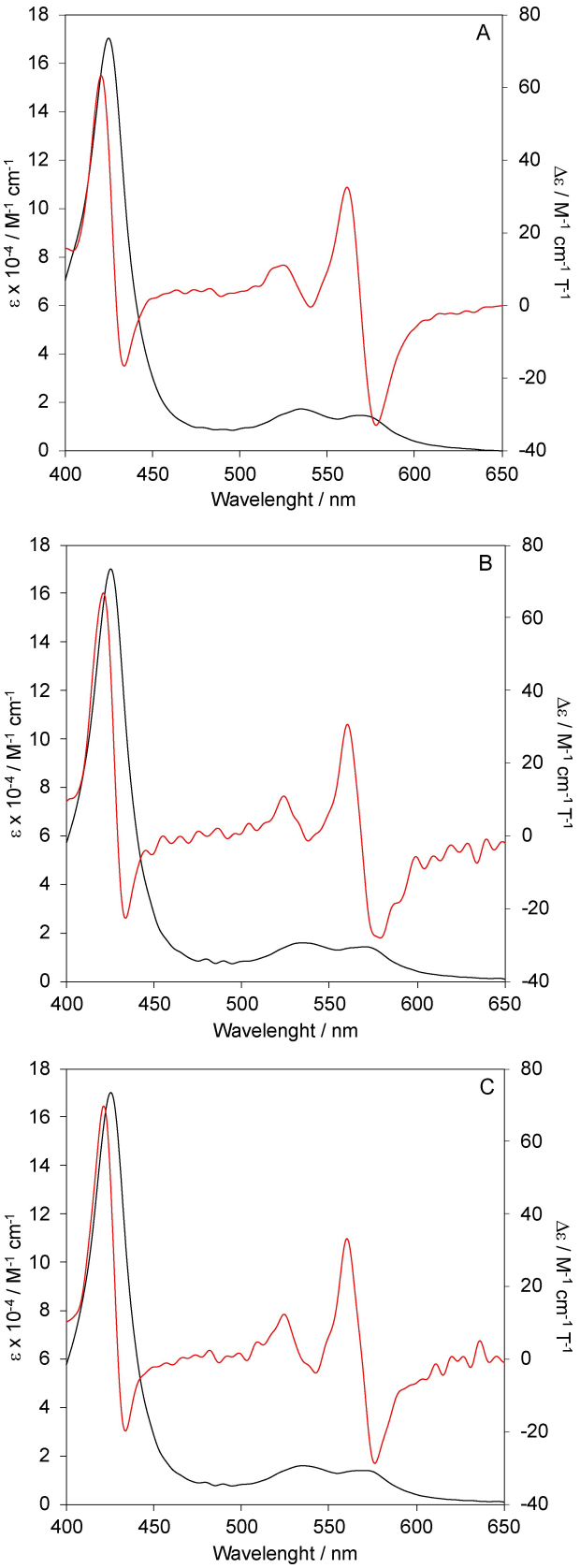

Figure 1. Electronic (black line, left y axis) and MCD (red line, right y axis) spectra of (A) Co–Mb; (B) Co–Mb adduct with NH_3; (C) Co–Mb adduct with imidazole. Protein solution was made up in 5 mM phosphate buffer and 50 mM sodium perchlorate pH = 7.2, T = 298 K.

of Co(III)-myoglobin (Figure 1A) features intense derivative-shaped signals in the correspondence of the Soret and α/β bands (Table 1) and is closely similar to those of low spin six-coordinated ferrous heme proteins, like cytochrome *c* and b_5 and the CO-adduct of ferrous myoglobin,[37,38] in agreement with the common $3d^6$ electronic configuration shared by low spin Co^{3+} and Fe^{2+}.[23,24]

Addition of imidazole and NH_3 to the protein solution results in a 1–3 nm red shift of electronic absorption and MCD signals (Figure 1B and 1C, Table 1). Therefore, it appears that both nitrogen ligands can replace the H_2O molecule as Co^{3+} distal axial ligand, without altering the low-spin state of the metal ion.

Thermodynamics and Kinetics for Heterogeneous Co–Mb Electron Transfer

After repeated (3–5) voltametric cycles, the CV of Co–Mb on a graphite electrode shows a well-defined quasi-reversible signal (Sg1) and two irreversible peaks at more cathodic potentials (Sg2 and Sg3) (Figure 2A and 3A).

Very similar responses were obtained also for the ammonia and imidazole adducts (Figure 2B, 2C and 3B, 3C). The CV of Co-protoporphyrin IX at the same pH shows only one irreversible cathodic peak at a more positive potential than those observed for Co–Mb (Figure 2D), indicating that the signals observed for Co–Mb

Table 1. Wavelengths of the relevant spectral bands in the UV-Vis and MCD spectra of Co(III)-substituted horse myoglobin and its imidazole and NH_3 adducts.

Co(III)-Mgb Wavelenghts at pH = 7.2												
Ligand	λ Uv-Vis/nm			2nd Deriv.	λ MCD/nm							
	Soret	β	α	Soret	Soret max	Soret min	Soret zerocross	β max	β min	α max	α min	α zerocross
H_2O	424	533	567	424	418	432	426	525	540	561	578	569
Imidazole	425	535	569	426	421	434	430	524	542	560	576	569
NH_3	425	534	570	425	421	434	429	524	538	560	579	568

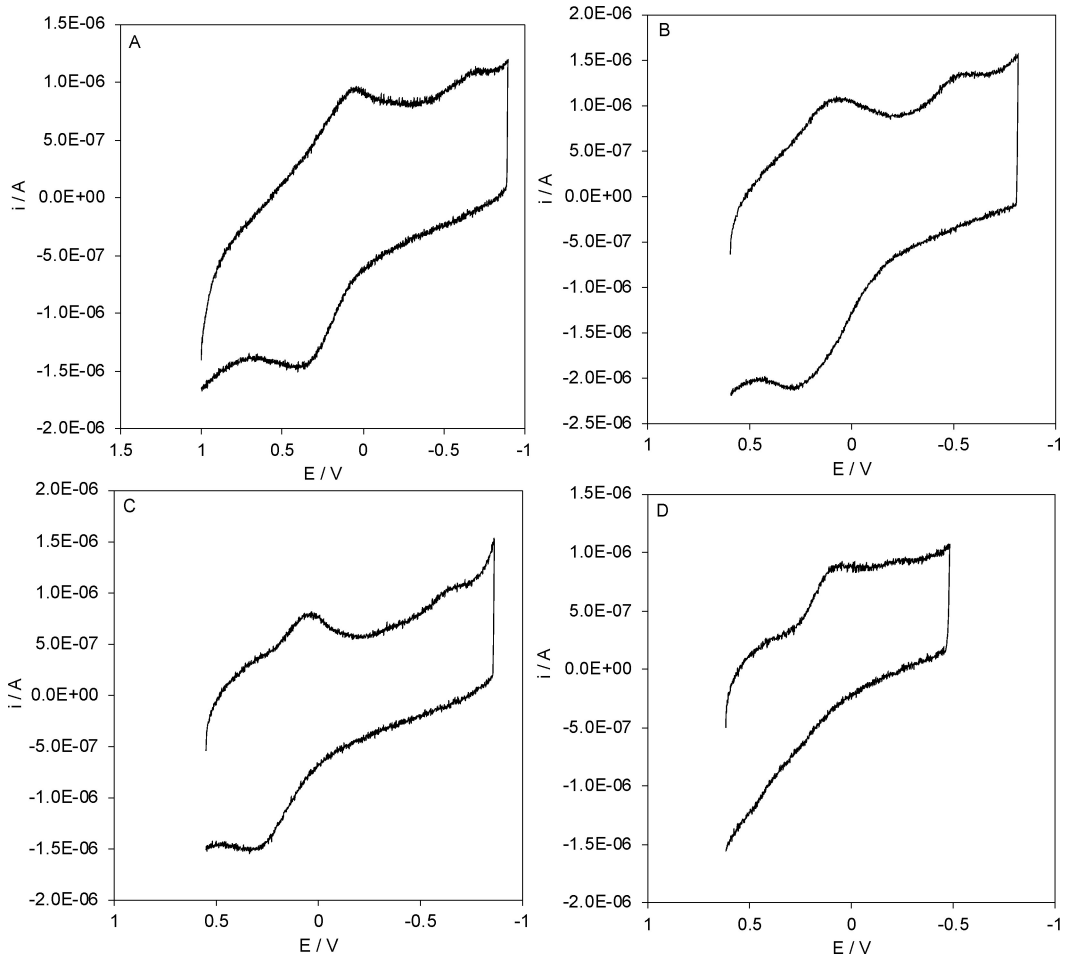

Figure 2. CV curves on graphite electrode (Sg1 and Sg2) for (A) Co–Mb; (B) Co–Mb adduct with NH_3; (C) Co–Mb adduct with imidazole; (D) cobalt protoporphyrin IX. Protein concentration, 3 μM; cobalt protoporphyrin IX concentration, about 2 μM; base electrolyte, 5 mM phosphate buffer plus 50 mM sodium perchlorate; pH = 7.2; T = 278 K.

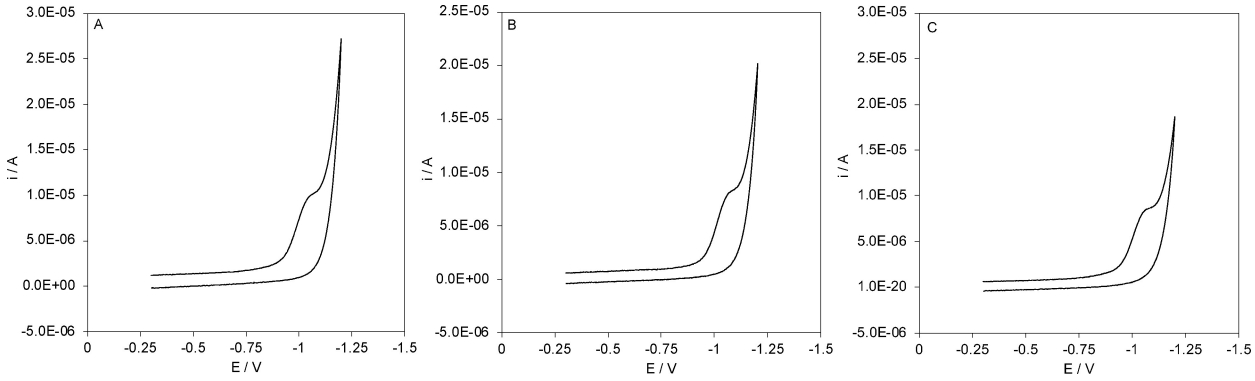

Figure 3. CV curves for the catalytical reduction of H_3O^+ (Sg3) at pH = 7.2 for (A) Co–Mb; (B) Co–Mb adduct with NH_3; (C) Co–Mb adduct with imidazole. Protein concentration, 3 μM; base electrolyte, 5 mM phosphate buffer plus 50 mM sodium perchlorate; pH = 7.2; T = 278 K.

and its derivatives originate from the Co-porphyrin center embedded into the protein catalytic pocket.

The signal Sg1 is typical of a quasi-reversible electrochemical process and consist of one cathodic peak along with its anodic counterpart. The $E^{\circ\prime}$ values of Sg1 together with E_{pc} of Sg2 and Sg3 for Co–Mb and its NH_3 and imidazole adducts at pH 7.2 are listed in Table 2.

For all species, the cathodic currents of Sg1 and Sg2 linearly increase with increasing *v*, as expected for an immobilized electroactive species, whereas that of Sg3 does not linearly increases with both v and $v^{1/2}$ (Figure 4). The peak-to-peak separation for Sg1 increases with increasing *v* and the $E^{\circ\prime}$ linearly decreases with increasing temperature.

Table 2. $E^{\circ\prime}$ value for reversible Sg1 and cathodic peak potentials (E_{pc}) for Sg1, Sg2 and Sg3 of Co–Mb and his adducts with ammonia and imidazole on a graphite electrode.[a]

	Co–Mb	Co–Mb + NH_3	Co–Mb + imidazole
$E^{\circ\prime}$(Sg1)/V	+0.205	+0.170	+0.174
E_{pc}(Sg1)/V	+0.032	+0.058	+0.040
E_{pc}(Sg2)/V	−0.695	−0.582	−0.656
E_{pc}(Sg3)/V	−1.066	−1.074	−1.081

[a] Base electrolyte, 5 mM phosphate buffer plus 50 mM sodium perchlorate, pH = 7.2, T = 298 K. Average errors on $E^{\circ\prime}$ and E_{pc} are ±0.004 V and ±0.002 V, respectively.

The plots of $E^{\circ\prime}$ *vs.* T for the Sg1 signal for Co–Mb and its adducts with ammonia and imidazole are reported in Figure 5 and the resulting thermodynamic parameters, $\Delta S^{\circ\prime}_{rc}$ and $\Delta H^{\circ\prime}_{rc}$, listed in Table 3. The electrochemical irreversibility of Sg2 and Sg3 prevents the determination of these parameters for the corresponding redox process. In the presence of dioxygen, the cathodic peak of Sg1 increases, while its anodic counterpart, Sg2 and Sg3 disappear.

The ET rate constants, k_s, of Co–Mb and its adducts were determined only for Sg1, which is the only signal showing adequate reversibility, using the Laviron method.[36] Measurements of k_s at varying temperature allowed determination of the activation enthalpy $\Delta H^{\#}$ and the pre-exponential factor for the ET process using the Arrhenius equation (Figure 6).

The resulting k_s and $\Delta H^{\#}$ values are of the same magnitude order of those determined for Fe–Mb immobilized on various functionalized electrodes.[39–42]

pH Dependence of E°

The $E^{\circ\prime}$ *vs* pH profiles for the Sg1 signal of Co–Mb and its NH_3 and imidazole adducts are shown in Figure 7. $E^{\circ\prime}$ is almost constant from pH 5.5 to 8 while it increases linearly below pH 5 with a slope of about 0.060 V per pH unit, suggesting the coupling of the reduction process with a proton uptake. Above pH 8, the $E^{\circ\prime}$ values decrease and do so more markedly at pH above 11. The electron

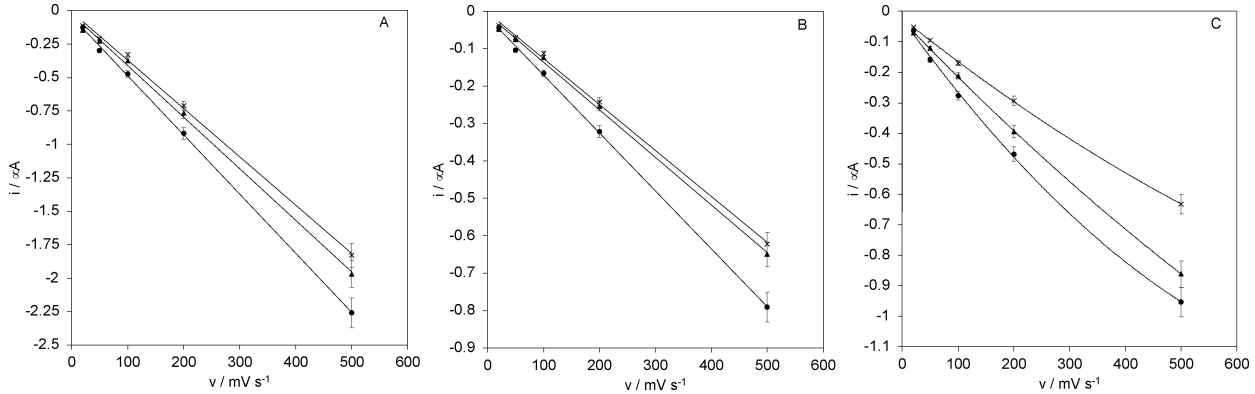

Figure 4. Plot of the cathodic peak currents of Sg1 (A), Sg2 (B) and Sg3 (C) *vs.* scan rate for Co–Mb (▲) and its adducts with ammonia (•) and imidazole (x). Base electrolyte, 5 mM phosphate buffer plus 50 mM sodium perchlorate; pH = 7.2; T = 298 K.

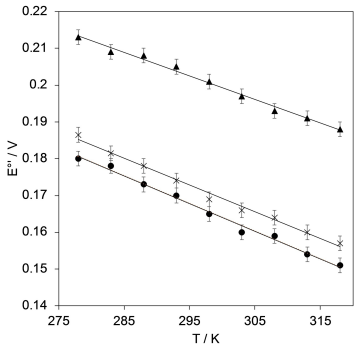

Figure 5. E°′ *vs.* T plot for the Sg1 signal of Co–Mb (▲) and its adducts with ammonia (•) and imidazole (×). Base electrolyte, 5 mM phosphate buffer plus 50 mM sodium perchlorate, pH = 7.2

Table 3. Thermodynamic ($\Delta S^{\circ\prime}_{rc}$ and $\Delta H^{\circ\prime}_{rc}$) and kinetic ($k_s$ at 298 K, $\Delta H^{\#}$ and lnA) parameters for the electron-transfer process associated to Sg1 for Co-myoglobin and his adducts with ammonia and imidazole on graphite electrode.[a]

Protein	$\Delta S^{\circ\prime}_{rc}$/ $Jmol^{-1}K^{-1}$	$\Delta H^{\circ\prime}_{rc}$/ $kJmol^{-1}$	k_s/ s^{-1}	$\Delta H^{\#}$/kJ mol^{-1}	lnA
Co–Mb	−62	−37.8	2.2	16.9	7.8
Co–Mb + NH_3	−73	−37.6	2.0	17.4	7.9
Co–Mb + im	−70	−37.4	4.8	15.1	7.8

[a] 5 mM phosphate buffer plus 50 mM sodium perchlorate, pH = 7.2. Average errors on $\Delta H^{\circ\prime}_{rc}$, $\Delta S^{\circ\prime}_{rc}$, k_s, $\Delta H^{\#}$ and lnA are ±0.3 kJ mol^{-1}, ±2 J $mol^{-1}K^{-1}$, ±6% (relative error), ±0.3 kJ mol^{-1} and ±0.02, respectively.

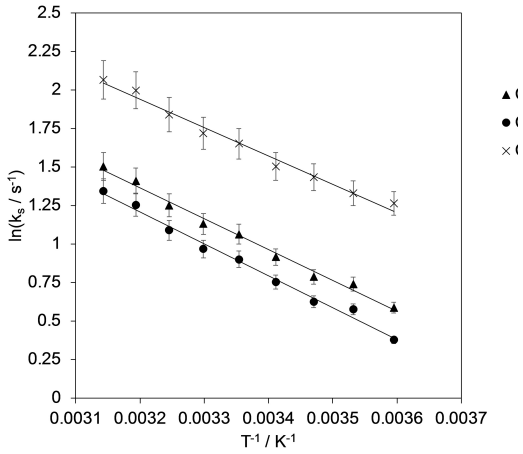

Figure 6. Arrhenius plots for the Sg1 signal of Co–Mb (▲) and its adducts with ammonia (•) and imidazole (×) on graphite electrode, pH = 7.2. Solid lines are least-squares fits to the data points.

transfer process in this pH region is therefore complex and probably involves structural modifications and/or unfolding of the protein.

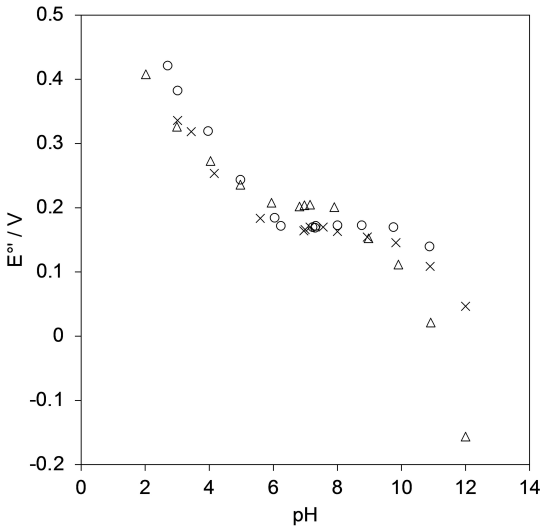

Figure 7. E°′ *vs.* pH profiles for the Sg1 signal of Co–Mb (△) and its adducts with NH_3 (○) and imidazole (×). T = 293 K.

Co–Mb Mediated Electrocatalytic Reduction of H_2O–H_3O^+ to H_2

The ability of Co–Mb and its NH_3 and imidazole adducts to catalyze the electrochemical reduction of H_3O^+ to H_2 was studied by cyclic voltammetry (CV) at different pH values. Co–Mb yields an intense catalytic wave at approximately −1.1 V in the CV curves (signal Sg3, Figure 3), covering the potential range corresponding to the reduction Co(I)/Co(0).[6] The catalytic current density *j* is strongly dependent on the pH, as expected for a molecular hydrogen-generating system (Figure 8). NH_3 and imidazole affect the response in a significant way inducing 20 mV cathodic shift of the onset potential of the catalytic wave and a decrease of the peak current (Figure 8).

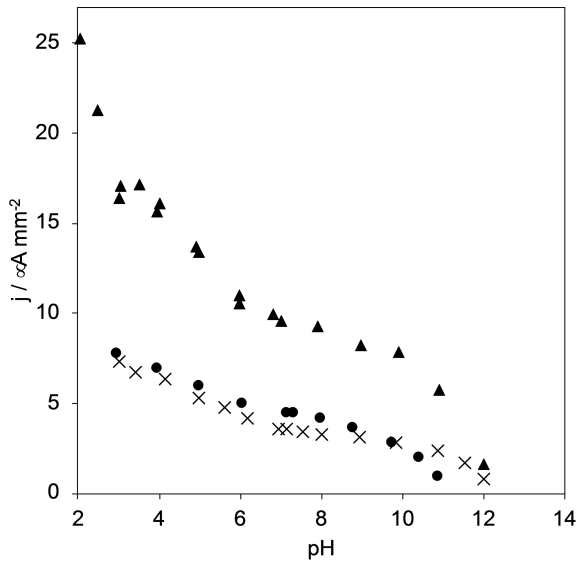

Figure 8. Plots of catalytic current density *j* *vs.* pH for Co–Mb (▲) and its adducts with ammonia (•) and imidazole (×). T = 293 K.

Discussion

The E°′ of Co–Mb

Freely diffusing Co–Mb does not show a well-defined voltammetric response on graphite electrode but does in the adsorbed phase on DDAB films.[43,44] In the present case, a reversible signal (Sg1) is obtained after a 3–5 CV cycles, most likely due to the formation of a protein film on the electrode that allows for efficient electron transfer between the adsorbed protein and the electrode surface. The resulting CV signals, that also include the irreversible peaks Sg2 and Sg3, are quite different from that of the Co-porphyrin complex. Therefore the electrochemical response is due to the Co(III)/Co(II) and Co(II)/Co(I) couples (*vide infra*) of the Co-protoporphyrin IX center bound to the protein matrix, although it cannot be excluded that the adsorption process causes conformational changes and/or partial leakage of the porphyrin group, as suggested by the width of the cathodic and anodic peaks.

The E°′ of Sg1 is about 100 mV more positive than that for the Co(III)/Co(II) couple of the protein in solution,[44] while the E_{pc} of Sg2 is about 70 mV more negative than that measured for the Co(II)/Co(I) pair of Co–Mb adsorbed on DDAB.[43] These results indicate that Sg1 and Sg2 are related to the Co(III)/Co(II) and the Co(II)/Co(I) couples of surface immobilized Co–Mb, respectively, while Sg3, whose current is strongly dependent of pH, is due to the catalytic reduction of the H_3O^+ species. Accordingly, in the presence of dioxygen the cathodic peak of Sg1 increase (owing to the catalytic reduction of dioxygen by Co(II) species generated by electrochemical reduction[45,46]), while its anodic counterpart, Sg2 and Sg3 disappear. The significant cathodic shift of the signal in the presence of NH_3 or imidazole is consistent with the replacement of the H_2O molecule acting as distal axial ligand in Co–Mb by the stronger N-donor ligands, which stabilizes the Co(III) state. Many ET proteins (ETP) adsorb onto neutral or ionic surface-modified electrodes,[47–52] often thanks to the same surface patch responsible for molecular recognition of the physiological partner(s). The redox properties of ETP are related to adsorption/interaction phenomena with surfaces or macromolecular systems (e.g. redox partners). As reported previously,[49,52,53] the interaction between the protein and ionic or neutral surfaces most often leads to an $E^{\circ\prime}$ shift indicating that the adsorption interaction stabilizes preferentially one of the two redox states.[31,54–58] Various factors contribute to differentiate the free energy in the two oxidation states of the protein, among which the alteration of the surface charge due to environmental factors (e.g. ions in solution, ionic strength), conformational changes and different interaction modes of the ox/red protein with the surface are the most relevant.[31,55–58] Graphite has a virtually neutral surface, but due to exposure to oxidizing solutions or simply to air, carboxyl and alcoholic groups are formed at the edge of the graphite sheet, capable of inducing significant adsorption capacities.[59–61] The resulting negative surface charge of graphite can determine a relevant contribution to E°′ (and ΔG°_{ads}). Although Co–Mb is negatively charged at pH 7.2, it can adsorb on the graphite electrode due to the presence of extensive positive surface domains (Figure 9), generating distinct signals related to consecutive oxidation/reduction processes of the metal center.

Comparison of the data in Table 2 with those reported in literature[44] reveals that the adsorption process induces a significant increase in $E^{\circ\prime}$ of the Co(III)/Co(II) couple (by about 100 mV). The primary binding interaction is probably electrostatic in nature. In our case it could involve surface lysine residues of the protein on one hand and the carboxylate groups of graphite on the other. Such an electrostatic adsorption should stabilize the less negatively charged oxidized Co(III)-Mb thereby resulting in a lower E°′ for signal Sg1 compared to the freely diffusing species. Therefore, the observed increase in E°′ is possibly due to a decrease in the exposure of the heme to the solvent following the adsorption on the electrode. Further contributions to E°′ from other adsorption-induced changes in the protein conformation cannot be excluded.

The cathodic peak potential of the Sg2 signal (Figure 2, Table 2) is attributed to the MbCo(II)→MbCo(I) reduction. The E_{pc} value of about 0.7 V for Co–Mb at pH 7 is in the same range of the formal potentials of MbCo(II)/MbCo(I) immobilized on DDAB[43] and the Co(II)L/Co(I)L redox couples of corrin and *salen* complexes in DDAB microemulsions.[62] The linear dependence of the peak current versus the scan rate shows that also this signal results from an adsorption-controlled process.

The signal Sg3, whose current is strongly dependent on pH, can be confidently attributed to the catalytic reduction of the H_3O^+ species, as the signal falls in a potential range similar to that usually reported for H_2 evolution catalyzed by Co-proteins and peptides.[6,14]

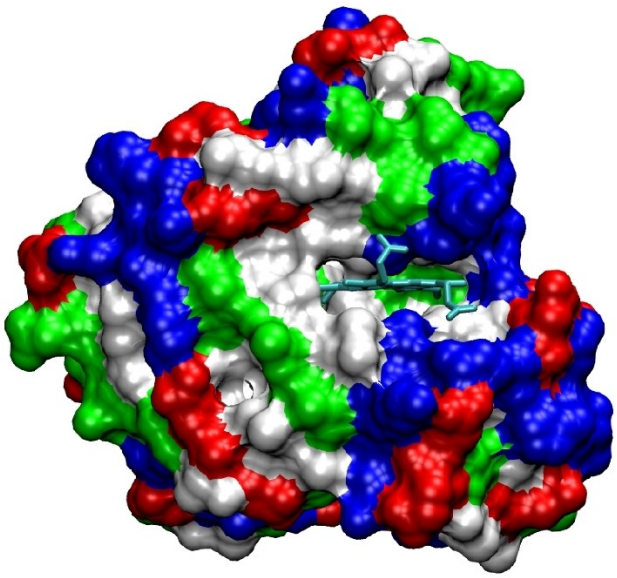

Figure 9. Cartoon representation (VMD Visual Molecular Dynamics, Humphrey, W., Dalke, A., Schulten, K., "VMD - Visual Molecular Dynamics", J. Molec. Graphics, 1996, vol. 14, pp. 33–38.) of the horse myoglobin structure (1WLA.pdb). The heme group is represented in light blue, whereas the acid, basic, polar and non-polar residues are represented in red, blue, green and white, respectively.

The Effect of pH on E°′ of Co–Mb

The E°′ value of a redox protein is most often affected by the solution pH. The pH indeed modifies the local and overall protonation state of the protein which in turn affect the electrostatic field acting on the redox center, modulated by charge distances, dielectric properties of the environment and solvation properties.[63,64] In turn, the redox state of the metal center affects the pK_a of the various acid-base residues. In the present case, the E°′ of Co(III)/Co(II)-Mb (signal Sg1) is influenced by at least two acid-base equilibria, at low and high pH values. On the basis of previous spectroscopic studies,[65] we can tentatively assign the equilibrium at acidic pH to the protonation of the two propionates of the tetrapyrrolic ring of Co-protoporphyrin IX. The acid/base equilibrium observed for Co–Mb at alkaline pH (>8) can instead be attributed to the deprotonation of the water molecule axially bound to Co(III) to yield an OH^- ion.[23,24] In the presence of NH_3 or imidazole as axial ligand, this acid/base equilibrium shifts at a much higher pH (>11) and is possibly related to the deprotonation of the imidazole ring of the vicinal axial histidine ligand.

The Reduction Thermodynamics of Co–Mb

The entropy ($\Delta S^{\circ\prime}_{rc}$) and enthalpy ($\Delta H^{\circ\prime}_{rc}$) changes associated with the reduction Co(III)/Co(II) in Co–Mb (signal Sg1) and in the corresponding NH_3 and imidazole adducts, in which the N-ligands replaced the water molecule as sixth (axial) ligand, were determined at pH 7.2 by measuring $E^{\circ\prime}$ as a function of temperature (Table 3). It turns out that axial ligand swapping remarkably affect the reduction thermodynamics.

The $\Delta S^{\circ\prime}_{rc}$ is negative for adsorbed Co–Mb regardless the nature of the axial ligand. The study of thermodynamic parameters associated with electron transfer processes allows important information to be gained on the factors that control the reduction potential in ETPs and redox metalloenzymes.[31,66–69] The remarkably positive value of E°′ for Co–Mb has an enthalpic origin. The negative value of $\Delta H^{\circ\prime}_{rc}$ is most likely related to the stabilization of Co(II) vs. Co(III) due to the partially hydrophobic environment and the poor basicity of the axial H_2O ligand. The negative entropic contribution (which, opposite to the enthalpic term, yields a negative contribution to E°′) is related to the reduction-induced changes in the hydrogen bond network at the protein-solution interface and in the ionic atmosphere (known cumulatively as "solvent reorganization effects") and to the variations in the flexibility of the polypeptide chain or parts of it,[31,66,68,70,71] which changes significantly due to H_2O swapping by the nitrogen-donor ligands. In general, the adsorbed proteins show negative $\Delta S^{\circ\prime}_{rc}$ values, as observed in the present case. A possible interpretation of these effects could be that the interaction of a more or less extensive region of the protein with the graphite surface via electrostatic interactions (involving the carboxylates and hydroxide groups formed upon oxidation) or van der Waals interactions causes the reorganization of the solvent at the contact region, thereby inducing significant conformational changes or hydrogen bond redistribution on the protein surface when the oxidation state of the metal center changes, as proposed for cytochrome *c* adsorbed on 1-mercapto-pyridine.[72] Surprisingly, $\Delta S^{\circ\prime}_{rc}$ and $\Delta H^{\circ\prime}_{rc}$ are not compensatory within the series including Co–Mb and its ammonia and imidazole adducts. Such compensation is observed when the enthalpy and entropy changes within the series are dominated by solvent reorganization effects, which involve intrinsically compensatory enthalpy and entropy changes.[31,73] In the present case the contribution of $\Delta H^{\circ\prime}_{rc}$ to E°′ does not change appreciably with changing the axial ligand, but $\Delta S^{\circ\prime}_{rc}$ does (Table 3). This indicates that the dominant contribution to the E°′ change following axial ligand replacement is yielded by the entropic component.

Kinetics of Heterogeneous Protein-Electrode ET for Electrode-Immobilized Co–Mb

The kinetics of the electron transfer process for electrode-immobilized Co–Mb and its axially ligated NH_3 and imidazole adducts, was studied by determining the electron transfer rate constant k_s at pH 7.2 at different temperatures using the approach developed by Laviron (Table 3).[36] Imidazole turns out not to significantly influence k_s, while NH_3 increases the rate of ET. This effect is due to a significant drop in $\Delta H^{\#}$, while the pre-exponential factor remains constant. This indicates that the geometric features of ET are unaffected by the axial ligand swapping, which instead lowers the reorganization energy.

The scarce efficiency of the heterogeneous ET for the protein is related to both a large activation barrier and pre-exponential factor. The large $\Delta H^{\#}$ could be attributed to the reduction induced distancing or dissociation of the axial ligand (water, NH_3 or imidazole). In the case of imidazole, the energy barrier of the ET process decreases. This effect can be put in relation with a different ability of imidazole to create a hydrogen bonding network involving the sixth axial heme cobalt ligand. The network of the hydrogen bonds around imidazole therefore turns out to facilitate heterogeneous ET with respect H_2O and NH_3.

According to the Marcus theory and considering that the k_s value obtained with the Laviron method corresponds to the electron transfer constant at zero driving force,[32,74] it can be shown that, upon assuming the activation entropy negligible, the k_s value can directly be related to the ET distance, r, by the equation:[32,74–77]

$$\ln k_s = \ln \nu_0 + [-\beta(r\text{-}r_0)] - \Delta G^{\#}/(RT)$$

In the present cases, using a β value of 1 $Å^{-1}$ and a frequency factor $\nu_0 = 6 \cdot 10^{12}\ s^{-1}$ (assumed to be kT/h), an $(r\text{-}r_0)$ value of about 15.4 Å is obtained. Therefore, if the above hypotheses are valid and estimating an r_0 value (nucleus-to-nucleus ET distance at donor-acceptor closest approach) of about 3 Å (generally used for Fe-heme[32,74–76]), in all cases the Co(III)/Co(II) metal center of the immobilized Co–Mb and its

ammonia and imidazole adducts turns out to be located about 12–13 Å from the electrode surface.

Electrocatalytic Reduction of H_3O^+ to H_2 by Electrode-Immobilized Co–Mb

At neutral pH and room temperature the onset potential for the reduction of H_3O^+ to H_2 on bare pyrolytic graphite electrode is observed at about −1.28 V (vs. SHE). In the presence of 3 μM Co–Mb under the same experimental conditions a new irreversible signal for the reduction of H_3O^+ to H_2 is observed featuring an onset potential of −0.92 V and a cathodic peak at about −1.08 V. The onset potential resembles that found for freely diffusing Co–Mb on glassy carbon,[6] suggesting that adsorption does not alter mechanism and efficiency of the catalytic reaction. The onset potential of the catalytic wave for the reduction of H_3O^+ to H_2 by immobilized Co–Mb results therefore about 0.36 V more positive than that of the same electrode in the absence of the protein. Similarly, onset potential values of −0.94 and −0.98 V are obtained for the imidazole and ammonia adducts of Co–Mb, respectively. Co–Mb and its adducts are therefore able to catalyze hydrogen reduction. This is in agreement with a previous work on Co-Mb,[6] suggesting a mechanism in which the reduction of Co(I) to Co(0) and a concerted PCET (Proton-Coupled Electron Transfer) lead to the catalytic production of H_2.[6,16,78,79] The onset potential for the catalytic wave of Co–Mb is approximately 20–50 mV more positive than that observed for water-soluble Co-porphyrins.[78] The onset potential is very similar to that already reported for free diffusing Co–Mb on glassy carbon at pH 7.5 under mild aerobic conditions.[6] In our case, however, the catalytic peak current is almost independent of the concentration of Co–Mb, indicating that the catalytic effect is (mainly) due to the adsorbed form of the protein. Moreover, the catalytic current is strongly dependent on the pH of the solution (Figure 8), as expected for the electrochemical processes of production of molecular hydrogen. Consecutive scans on Co–Mb at pH 7.2 showed no significant drop in catalytic current. The CVs were also repeated in open electrochemical cell condition (i.e., exposed to the atmosphere), observing a loss of catalytic current. Similar behaviors are also shown by the NH_3 and imidazole adducts.

The electrocatalytic current density (*j*) of Co–Mb and its adducts with N-donors at different pH values (Figure 8) show that the best catalytic efficiency is yielded by Co–Mb. Imidazole and NH_3 axial ligation induces a significant decrease in the *j* values. Nitrogenous ligands, therefore, directly affect the catalytic mechanism, yielding a remarkable efficiency decrease.

Since the Co(III)/Co(II) reduction currents are very similar for Co–Mb and its adducts, the drop in current density is not attributable to a different surface concentration of the protein (catalyst) on the electrode surface. It is likely that the exogenous axial ligand limits the accessibility of the substrate (water) to the heme Co center for steric reasons or because it modifies the H-bond network in the catalytic pocket or simply disfavors the reduction of Co(I) to Co(0).

Table 4. Catalytic parameters of H_2 evolving for the investigated proteins and some selected Co-porphyrin/peptide electrocatalysts.

	pH	Onset potential[a]/V	Overpotential[a]/V	longevity[b]/V
Co-substituted MP11[c]	7	−0.98	0.852	0.4
MC6*a[d]	6.5	−0.87	0.680	1.4
Ht–CoM61A[e]	7	−1.07	0.830	6
Co–Mb	7.2	−0.92	0.608	2.5
Co–Mb + Imidazole	7.2	−0.94	0.622	3.1
Co–Mb + NH_3	7.2	−0.98	0.646	3.3

[a] Calculated as reported in [14]. [b] Calculated as the electrolysis time to the catalytic peak that retains 80% of the catalytic signal in CV. [c] From ref. [7]. [d] From ref. [14]. [e] From ref. [12].

Selected catalytic properties of the studied proteins have been calculated and reported in Table 4 together with those of Co-adducts of some heme proteins and peptides that have similar metal center structures.[7,12,14] Co–Mb and its adducts show onset potential and overpotential similar or even lower than those of other known Co-porphyrin/polypeptide electrocatalysts. In particular, the performance of Co–Mb is completely comparable with MC6*a, which is one of the most efficient polypeptides for the production of H_2 at pH around neutrality. Unlike the latter system, however, Co–Mb is rather sensitive to the presence of O_2, likely due to the greater exposure of Co-heme. Such sensitivity persists also in the presence of exogenous ligands such as imidazole and ammonia. Rationally-designed point mutations on Mb that would reduce the exposure of the Co-heme center to solvent could solve this problem. The longevity of the catalytic properties of Co–Mb appears to be rather high, although somewhat lower than that of Ht-CoM61A which shows a particularly high catalytic stability thanks to a metal center rather hidden inside the protein structure.

Conclusions

We exploited electrode-immobilized Co-substituted myoglobin, a heme oxygen-transfer protein, to electrochemically catalyze H_2 production in the adsorbed state. The catalytic efficiency is modulated by the nature of the exogenous axial ligand and decreases in the presence of dioxygen, whose reduction is in turn activated by the reduction of Co(III) to Co(II). Upon adsorption on the pyrolytic graphite electrode, Co-substituted Mb is therefore capable of producing H_2 in aqueous solution, a property not common to cobalt catalysts for hydrogen production. Since the present system is efficient, stable and reproducible, it offers the possibility of scalable electrocatalysis and can be produced in quantities with a relatively simple procedure.

Abbreviations

Mb	horse myoglobin
Co-Mb	cobalt substituted myoglobin
CV	cyclic voltammetry

Acknowledgements

Funding information: This work was supported by the University of Modena and Reggio Emilia FAR Mission Oriented 2022 (Cobalt-substituted globins as catalysts for electrochemical hydrogen production – GB) funding program and by EU – NextGenerationEU - PIANO NAZIONALE DI RIPRESA E RESILIENZA (PNRR) – MISSIONE 4 COMPONENTE 2, "Dalla ricerca all'impresa" INVESTIMENTO 1.5, "Creazione e rafforzamento di "Ecosistemi dell'innovazione" costruzione di "leader Territoriali di R&S" finanziato dall'Unione europea – NextGenerationEU" - Progetto identificato con codice ECS00000033 – Titolo "Ecosystem for Sustainable Transition in Emilia-Romagna – Avviso MUR DD 3277/2021.

The text describes the ideas and the opinions of the authors, which do not necessarily reflect those of the EU and European Commission. Nor EU neither European Commission can be considered responsible for the content of the manuscript.

Conflict of Interests

The authors declare that they have no known competing financial interests or personal relationships that could have appeared to influence the work reported in this paper.

Data Availability Statement

The data that support the findings of this study are available from the corresponding author upon reasonable request.

Keywords: myoglobin · cobalt protoporphyrin IX · electron transfer · hydrogen production · bio-electrocatalysis

[1] M. Momirlan, T. N. Veziroglu, *Int. J. Hydrogen Energy* **2005**, *30*, 795–802.
[2] P. P. Edwards, V. L. Kuznetsov, W. I. F. David, N. P. Brandon, *Energy Policy* **2008**, *36*, 4356–4362.
[3] D. Dolui, S. Das, J. Bharti, S. Kumar, P. Kumar, A. Dutta, *Cell Rep. Phys. Sci.* **2020**, *1*, 100007.
[4] W. Lubitz, H. Ogata, O. Rüdiger, E. Reijerse, *Chem. Rev.* **2014**, *114*, 4081–4148.
[5] A. Onoda, T. Hayashi, *Curr. Opin. Chem. Biol.* **2015**, *25*, 133–140.
[6] D. J. Sommer, M. D. Vaughn, G. Ghirlanda, *Chem. Commun.* **2014**, *50*, 15852–15855.
[7] J. G. Kleingardner, B. Kandemir, K. L. Bren, *J. Am. Chem. Soc.* **2014**, *136*, 4–7.
[8] G. M. Jacobsen, J. Y. Yang, B. Twamley, A. D. Wilson, R. M. Bullock, M. Rakowski Dubois, D. L. Dubois, *Energy Environ. Sci.* **2008**, *1*, 167–174.
[9] M. Bacchi, G. Berggren, J. Niklas, E. Veinberg, M. W. Mara, M. L. Shelby, O. G. Poluektov, L. X. Chen, D. M. Tiede, C. Cavazza, M. J. Field, M. Fontecave, V. Artero, *Inorg. Chem.* **2014**, *53*, 8071–8082.
[10] B. Kandemir, L. Kubie, Y. Guo, B. Sheldon, K. L. Bren, *Inorg. Chem.* **2016**, *55*, 1355–1357.
[11] Y. Guo, J. R. Stroka, B. Kandemir, C. E. Dickerson, K. L. Bren, *J. Am. Chem. Soc.* **2018**, *140*, 16888–16892.
[12] B. Kandemir, S. Chakraborty, Y. Guo, K. L. Bren, *Inorg. Chem.* **2016**, *55*, 467–477.
[13] L. Leone, G. Sgueglia, S. La Gatta, M. Chino, F. Nastri, A. Lombardi, *Int. J. Mol. Sci.* **2023**, *24*, 8605.
[14] V. Firpo, J. M. Le, V. Pavone, A. Lombardi, K. L. Bren, *Chem. Sci.* **2018**, *9*, 8582–8589.
[15] A. D. Wilson, R. H. Newell, M. J. McNevin, J. T. Muckerman, M. Rakowski DuBois, D. L. DuBois, *J. Am. Chem. Soc.* **2006**, *128*, 358–366.
[16] C. H. Lee, D. K. Dogutan, D. G. Nocera, *J. Am. Chem. Soc.* **2011**, *133*, 8775–8777.
[17] X. Hu, B. S. Brunschwig, J. C. Peters, *J. Am. Chem. Soc.* **2007**, *129*, 8988–8998.
[18] O. Daltrop, S. J. Ferguson, *J. Biol. Chem.* **2004**, *279*, 45347–45353.
[19] T. Yonetani, *J. Biol. Chem.* **1967**, *242*, 5008–5013.
[20] T. Yonetani, T. Asakura, *J. Biol. Chem.* **1969**, *244*, 4580–4588.
[21] T. Yonetani, H. Yamamoto, G. V. Woodrow, *J. Biol. Chem.* **1974**, *249*, 682–90.
[22] M. C. Marden, L. Kiger, C. Poyart, A. K. Rashid, J. Kister, F. Stetzkowski-Marden, G. Caron, M. Haque, L. Moens, *FEBS Lett.* **2000**, *472*, 221–224.
[23] S. Neya, M. Suzuki, T. Hoshino, A. T. Kawaguchi, *Inorg. Chem.* **2013**, *52*, 7387–7393.
[24] S. Neya, T. Yonetani, A. T. Kawaguchi, *Artif. Organs* **2014**, *38*, 715–719.
[25] F. W. Snyder, J. C. W. Chien, *J. Mol. Biol.* **1979**, *135*, 315–325.
[26] F. Paulat, N. Lehnert, *Inorg. Chem.* **2008**, *47*, 4963–4976.
[27] M. Bellei, C. A. Bortolotti, G. Di Rocco, M. Borsari, L. Lancellotti, A. Ranieri, M. Sola, G. Battistuzzi, *J. Inorg. Biochem.* **2018**, *178*, 70–86.
[28] G. Di Rocco, G. Battistuzzi, C. A. Bortolotti, M. Borsari, E. Ferrari, S. Monari, M. Sola, *J. Biol. Inorg. Chem.* **2011**, *16*, 461–471.
[29] E. L. Yee, M. J. Weaver, *Inorg. Chem.* **1980**, *19*, 1077–1079.
[30] E. L. Yee, R. J. Cave, K. L. Guyer, P. D. Tyma, M. J. Weaver, *J. Am. Chem. Soc.* **1979**, *101*, 1131–1137.
[31] G. Di Rocco, G. Battistuzzi, M. Borsari, C. A. Bortolotti, A. Ranieri, M. Sola, *Coord. Chem. Rev.* **2021**, *445*, 214071.
[32] S. Song, R. A. Clark, E. F. Bowden, M. J. Tarlov, *J. Phys. Chem.* **1993**, *97*, 6564–6572.
[33] S. Monari, A. Ranieri, C. A. Bortolotti, S. Peressini, C. Tavagnacco, M. Borsari, *Electrochim. Acta* **2011**, *56*, 6925–6931.
[34] A. Ranieri, G. Battistuzzi, M. Borsari, C. A. Bortolotti, G. Di Rocco, S. Monari, M. Sola, *Electrochem. Commun.* **2012**, *14*, 29–31.
[35] M. Gómez-Mingot, V. Montiel, C. E. Banks, J. Iniesta, *Analyst* **2014**, *139*, 1442–1448.
[36] E. Laviron, *J. Electroanal. Chem. Interfacial Electrochem.* **1979**, *101*, 19–28.
[37] L. Vickery, T. Nozawa, K. Sauer, *J. Am. Chem. Soc.* **1976**, *98*, 343–350.
[38] L. Vickery, T. Nozawa, K. Sauer, *J. Am. Chem. Soc.* **1976**, *98*, 351–357.
[39] C. N. Toledo, F. H. Florenzano, J. M. Schneedorf, *Int. J. Electrochem.* **2014**, *2014*, 1–7.
[40] B. R. Van Dyke, P. Saltman, F. A. Armstrong, *J Am Chem Soc* **1996**, *118*, 3490–3492.
[41] S. Boussaad, N. J. Tao, *J. Am. Chem. Soc.* **1999**, *121*, 4510–4515.
[42] D. E. Khoshtariya, T. D. Dolidze, M. Shushanyan, R. Van Eldik, *J. Phys. Chem. B* **2014**, *118*, 692–706.
[43] J. Gao, J. F. Rusling, *J. Electroanal. Chem.* **1998**, *449*, 1–4.
[44] C. Li, K. Nishiyama, I. Taniguchi, *Electrochim. Acta* **2000**, *45*, 2883–2888.
[45] S. Gupta, R. Fernandes, R. Patel, M. Spreitzer, N. Patel, *Appl. Catal. A* **2023**, *661*, 119254.
[46] Y. H. Wang, M. L. Pegis, J. M. Mayer, S. S. Stahl, *J. Am. Chem. Soc.* **2017**, *139*, 16458–16461.
[47] D. Gopal, G. S. Wilson, R. A. Earl, M. A. Cusanovich, *J. Biol. Chem.* **1988**, *263*, 11652–11656.
[48] A. El Kasmi, J. M. Wallace, E. F. Bowden, S. M. Binet, R. J. Linderman, *J. Am. Chem. Soc.* **1998**, *120*, 225–226.
[49] G. Gavioli, M. Borsari, M. Cannio, A. Ranieri, G. Volponi, *J. Electroanal. Chem.* **2004**, *564*, 45–52.
[50] M. Hromadová, W. R. Fawcett, *J. Phys. Chem. B* **2004**, *108*, 3277–3282.
[51] D. Millo, A. Bonifacio, A. Ranieri, M. Borsari, C. Gooijer, G. Van Der Zwan, *Langmuir* **2007**, *23*, 4340–4345.
[52] J. L. Willit, E. F. Bowden, *J. Phys. Chem.* **1990**, *94*, 8241–8246.
[53] Z. Salamon, G. Tollin, *J. Bioenerg. Biomembr.* **1997**, *29*, 211–221.
[54] G. Battistuzzi, M. Borsari, M. Sola, *Antioxid. Redox Signaling* **2001**, *3*, 279–291.
[55] C. Léger, P. Bertrand, *Chem. Rev.* **2008**, *108*, 2379–2438.

[56] D. H. Murgida, P. Hildebrandt, *Phys. Chem. Chem. Phys.* **2005**, *7*, 3773.
[57] F. A. Armstrong, G. S. Wilson, *Electrochim. Acta* **2000**, *45*, 2623–2645.
[58] N. D. J. Yates, M. A. Fascione, A. Parkin, *Chem. - Eur. J.* **2018**, *24*, 12164–12182.
[59] R. E. Panzer, P. J. Elving, *Electrochim. Acta* **1975**, *20*, 635–647.
[60] K. F. Blurton, *Electrochim. Acta* **1973**, *18*, 869–875.
[61] M. X. Qiao, Y. Zhang, L. F. Zhai, M. Sun, *Chem. Eng. J.* **2018**, *344*, 410–418.
[62] D. Zhou, J. Gao, J. F. Rusling, *J. Am. Chem. Soc.* **1995**, *117*, 1127–1134.
[63] R. A. Scott, A. G. Mauk, *Cytochrome c-A Multidisciplinary Approach*, University Science Books, Sausalito (CA), **1996, 1-738**.
[64] G. R. Moore, G. W. Pettigrew, *Cytochromes c*, Springer Berlin Heidelberg, Berlin, Heidelberg, **1990**, pp 1–478.
[65] S. Mathura, D. Sannasy, A. S. De Sousa, C. B. Perry, I. Navizet, H. M. Marques, *J. Inorg. Biochem.* **2013**, *123*, 66–79.
[66] G. Battistuzzi, M. Borsari, M. Sola, *Eur. J. Inorg. Chem.* **2001**, 2989–3004.
[67] G. Battistuzzi, M. Borsari, J. A. Cowan, C. Eicken, L. Loschi, M. Sola, *Biochemistry* **1999**, *38*, 5553–5562.
[68] P. Bertrand, O. Mbarki, M. Asso, L. Blanchard, F. Guerlesquin, M. Tegoni, *Biochemistry* **1995**, *34*, 11071–11079.
[69] S. Benini, M. Borsari, S. Ciurli, A. Dikiy, M. Lamborghini, *JBIC J. Biol. Inorg. Chem.* **1998**, *3*, 371–382.
[70] G. Battistuzzi, M. Borsari, M. Sola, F. Francia, *Biochemistry* **1997**, *36*, 16247–16258.
[71] K. B. Koller, F. M. Hawkridge, *J. Am. Chem. Soc.* **1985**, *107*, 7412–7417.
[72] A. Szucs, G. D. Hitchens, J. O. Bockris, *Electrochim. Acta* **1992**, *37*, 403–412.
[73] G. Battistuzzi, M. Borsari, G. Di Rocco, A. Ranieri, M. Sola, *J. Biol. Inorg. Chem.* **2004**, *9*, 23–26.
[74] M. J. Tarlov, E. F. Bowden, *J. Am. Chem. Soc.* **1991**, *113*, 1847–1849.
[75] R. A. Marcus, N. Sutin, *Biochim. Biophys. Acta* **1985**, *811*, 265–322.
[76] S. Casalini, G. Battistuzzi, M. Borsari, C. A. Bortolotti, G. Di Rocco, A. Ranieri, M. Sola, *J. Phys. Chem. B* **2010**, *114*, 1698–1706.
[77] S. Monari, G. Battistuzzi, C. A. Bortolotti, S. Yanagisawa, K. Sato, C. Li, I. Salard, D. Kostrz, M. Borsari, A. Ranieri, C. Dennison, M. Sola, *J. Am. Chem. Soc.* **2012**, *134*, 11848–11851.
[78] M. Natali, A. Luisa, E. Iengo, F. Scandola, *Chem. Commun.* **2014**, *50*, 1842–1844.
[79] J. T. Muckerman, E. Fujita, *Chem. Commun.* **2011**, *47*, 12456–12458.

Manuscript received: December 19, 2023
Revised manuscript received: February 5, 2024
Version of record online: March 13, 2024